JACS
JOURNAL OF THE AMERICAN CHEMICAL SOCIETY
pubs.acs.org/JACS
Article

Achieving High-Efficient Photoelectrocatalytic Degradation of 4-Chlorophenol via Functional Reformation of Titanium-Oxo Clusters

Jing-Jing Liu, Sheng-Nan Sun, Jiang Liu,* Yi Kuang, Jing-Wen Shi, Long-Zhang Dong, Ning Li, Jia-Ni Lu, Jiao-Min Lin, Shun-Li Li, and Ya-Qian Lan*

Cite This: J. Am. Chem. Soc. 2023, 145, 6112−6122
Read Online

ABSTRACT: Rational design of crystalline catalysts with superior light absorption and charge transfer for efficient photoelectrocatalytic (PEC) reaction coupled with energy recovery remains a great challenge. In this work, we elaborately construct three stable titanium-oxo clusters (TOCs, $Ti_{10}Ac_6$, $Ti_{10}Fc_8$, and $Ti_{12}Fc_2Ac_4$) modified with a monofunctionalized ligand (9-anthracenecarboxylic acid (Ac) or ferrocenecarboxylic acid (Fc)) and bifunctionalized ligands (Ac and Fc). They have tunable light-harvesting and charge transfer capacities and thus can serve as outstanding crystalline catalysts to achieve efficient PEC overall reaction, that is, the integration of anodic organic pollutant 4-chlorophenol (4-CP) degradation and cathodic wastewater-to-H_2 conversion. These TOCs can all exhibit very high PEC activity and degradation efficiency of 4-CP. Especially, $Ti_{12}Fc_2Ac_4$ decorated with bifunctionalized ligands exhibits better PEC degradation efficiency (over 99%) and H_2 generation than $Ti_{10}Ac_6$ and $Ti_{10}Fc_8$ modified with a monofunctionalized ligand. The study of the 4-CP degradation pathway and mechanism revealed that such better PEC performance of $Ti_{12}Fc_2Ac_4$ is probably due to its stronger interactions with the 4-CP molecule and better $^{\bullet}OH$ radical production. This work not only presents the effective combination of organic pollutant degradation and simultaneously H_2 evolution reaction using crystalline coordination clusters as both anodic and cathodic catalyst but also develops a new PEC application for crystalline coordination compounds.

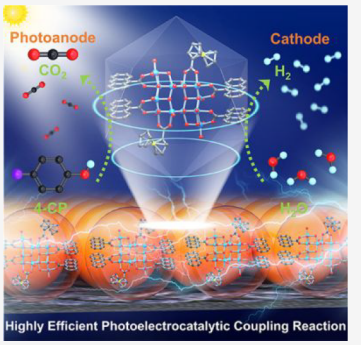

INTRODUCTION

With the rapid development of global industrialization, water pollution has been recognized as one of the most prominent global environmental deterioration problems.[1−3] In particular, wastewater containing widely used but refractory organic pollutants (e.g., phenolic compounds) is directly discharged into the environment, which poses a serious threat to human health.[4,5] 4-Chlorophenol (4-CP) is one of the common toxic and low biodegradable phenolic organic pollutants.[6] It is widely used in large-scale disinfection of drinking water, pesticide production, and natural chlorination of organic substances, which has long-term harmful effects on people's daily lives.[7] Currently, the treatment methods of the organic pollutant 4-CP in water mainly include traditional biological treatment,[8] piezo-catalytic,[9] adsorption,[10] microwave-enhanced catalytic,[11] and other technologies.[12,13] However, these treatment technologies have some drawbacks, such as long and incomplete degradation cycles, high energy consumption, high costs, and even causing secondary chlorination of organic substances, which significantly limits their applications in the field of water purification.[14] Besides, many of these technologies neglect that there is a large amount of chemical energy (e.g., H_2 energy) in wastewater, Therefore, it is urgent to develop more efficient and ecofriendly technologies for the treatment of organic pollutants and the comprehensive utilization of chemical energy.

Photoelectrocatalytic (PEC) degradation technology, which combines the benefits of photocatalysis and electrocatalysis, offers a very promising approach for efficiently removing refractory organic pollutants from wastewater systems.[15,16] In addition, this technology can in theory simultaneously achieve pollutant degradation and clean energy production through overall reaction, that is, the integration of anodic organic pollutant degradation coupled with cathodic wastewater-to-H_2 reduction.[17] Importantly, such a PEC overall reaction can realize both wastewater purification and energy recovery.[18] Moreover, if a material can be used as both an anodic and cathodic catalyst to accomplish this overall reaction, it will be more attractive in terms of reducing catalytic cost and simplifying electrolysis devices.[19] Nevertheless, the design and synthesis of such PEC overall reaction catalysts still

Received: October 30, 2022
Published: March 8, 2023

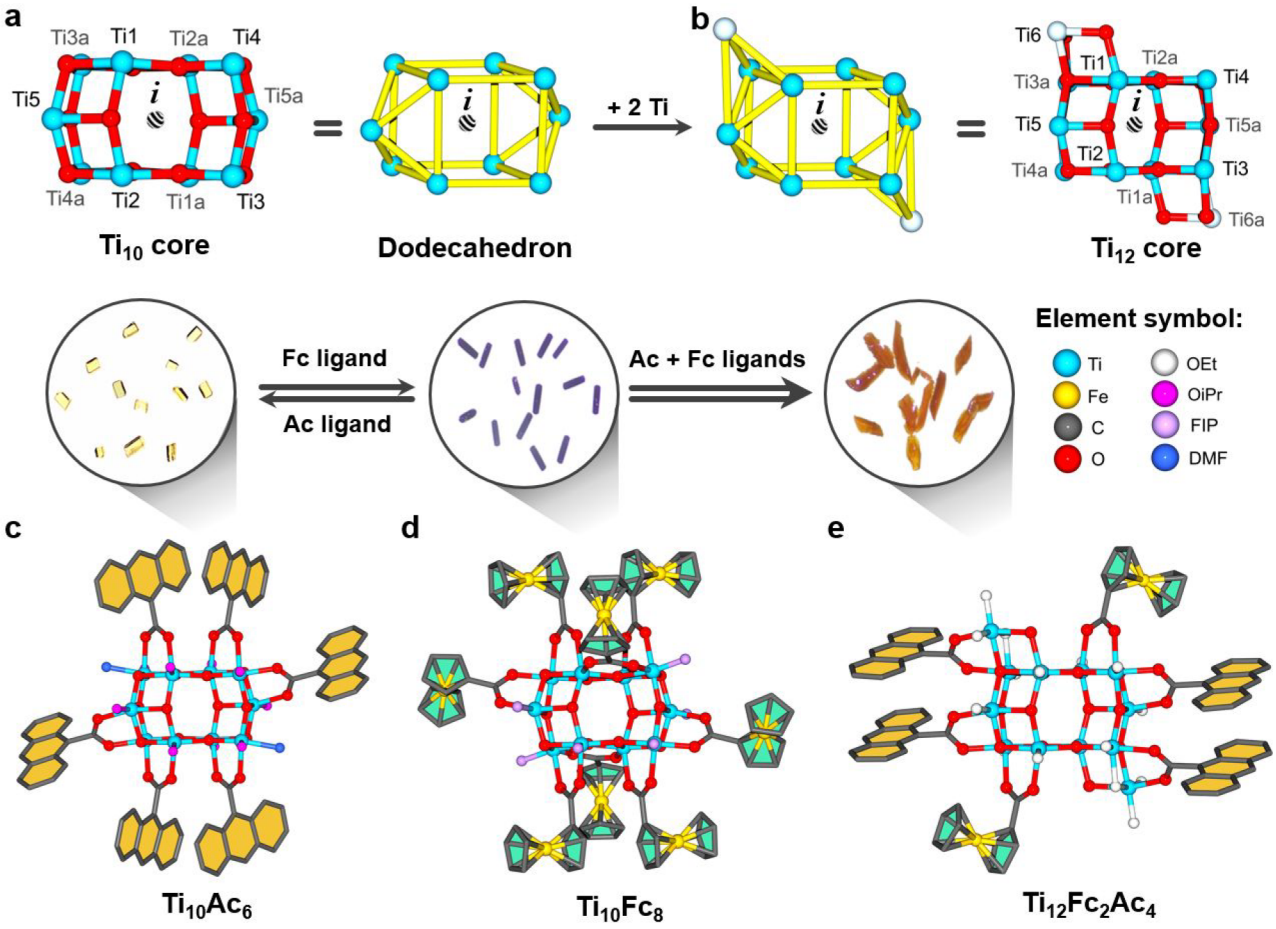

Figure 1. (a) The $\{Ti_{10}\}$ metal-oxo core and dodecahedron skeleton of $\mathbf{Ti_{10}Ac_6}$ and $\mathbf{Ti_{10}Fc_8}$.The striped ball represents the inversion center (i). (b) The $\{Ti_{12}\}$ metal-oxo core of $\mathbf{Ti_{12}Fc_2Ac_4}$. The $\{Ti_{12}\}$ core is equal to a $\{Ti_{10}\}$ core bridged by two additional symmetric Ti6 atoms. (c, d, e) The whole molecular structures of $\mathbf{Ti_{10}Ac_6}$, $\mathbf{Ti_{10}Fc_8}$, and $\mathbf{Ti_{12}Fc_2Ac_4}$. These clusters are made up of a $\{Ti_{10}\}/\{Ti_{12}\}$ core and mono/bifunctionalized organic ligands (Ac and Fc). In the middle of the picture, the crystal photographs of $\mathbf{Ti_{10}Ac_6}$, $\mathbf{Ti_{10}Fc_8}$, and $\mathbf{Ti_{12}Fc_2Ac_4}$ under an optical microscope are presented. All hydrogen atoms are omitted for clarity. Ac = 9-anthracenecarboxylic acid, Fc = ferrocenecarboxylic acid, O^iPr = isopropanol, DMF = *N*,*N*-dimethylformamide, FIP = hexafluoroisopropanol, OEt = ethanol. Color codes: sky blue = Ti atoms, light blue = Ti6 atom, orange = Fe atoms, dark gray = C atoms, red = O atoms, light gray = OEt molecules, pink = O^iPr molecules, purple = FIP molecules, light blue = DMF molecules.

remains a great challenge.[20] Coordination compounds, which are crystalline materials formed by periodical linking metal ions or metal cluster centers with functionalized organic ligands, offer a great potential platform for the exploration of a PEC overall reaction catalyst.[21−24] On one hand, their clear structural information can accurately identify catalytic active sites and establish structure−activity relationships when they are used as catalysts.[25−27] On the other hand, their structures and properties can be modulated via specific functional organic ligands.[28−31] Nevertheless, their application in the field of PEC overall reaction is still very scarce.

Herein, we designed and synthesized three stable titanium-oxo clusters (TOCs): $Ti_{10}(\mu_3\text{-}O)_{12}(Ac)_6(O^iPr)_{10}(DMF)_2$ ($\mathbf{Ti_{10}Ac_6}$; Ac = 9-anthracenecarboxylic acid, O^iPr = isopropanol, and DMF = *N*,*N*-dimethylformamide), $Ti_{10}(\mu_3\text{-}O)_{12}(Fc)_8(FIP)_8$ ($\mathbf{Ti_{10}Fc_8}$; Fc = ferrocenecarboxylic acid and FIP = hexafluoroisopropanol), and $Ti_{12}(\mu_4\text{-}O)_2(\mu_3\text{-}O)_{10}(\mu_2\text{-}OEt)_4(Ac)_4(Fc)_2(OEt)_{14}$ ($\mathbf{Ti_{12}Fc_2Ac_4}$; OEt = ethanol), which can be utilized as crystalline bifunctional catalysts for both photoanodes and cathodes to realize the high-efficiency removal of the persistent organic pollutant 4-CP coupled with wastewater-to-H_2 conversion. Owing to the modification of Fc (featuring redox properties and the fast charge transfer capability) and Ac ligands (a rigid conjugation plane),[32,33] these three TOCs exhibit significantly enhanced light absorption and charge transfer capabilities. Therefore, when these clusters are used for PEC degradation of the organic pollutant 4-CP, they can exhibit high PEC activity and degradation rate. Especially, $\mathbf{Ti_{12}Fc_2Ac_4}$ modified with bifunctionalized ligands exhibits better PEC degradation efficiency (over 99%) and H_2 generation than $\mathbf{Ti_{10}Ac_6}$ and $\mathbf{Ti_{10}Fc_8}$ modified with a monofunctionalized ligand. In addition, the PEC degradation pathway and mechanism of the pollutant 4-CP were studied by combining high-performance liquid chromatography and electron paramagnetic resonance spectra. This work not only presents a PEC tandem reaction for the degradation of the contaminant 4-CP in wastewater and wastewater-to-H_2 conversion effectively using one crystalline coordination compound as anodic and cathodic catalyst, but also provides additional insight into the rational design and construction of more efficient crystalline coordination compound catalysts for the efficient PEC wastewater purification and energy recovery.

https://doi.org/10.1021/jacs.2c11509
J. Am. Chem. Soc. 2023, 145, 6112−6122

RESULTS AND DISCUSSION

$Ti_{10}Ac_6$, $Ti_{10}Fc_8$, and $Ti_{12}Fc_2Ac_4$ crystals (Figure 1) were synthesized by the in situ solvothermal synthesis method in high yields (see the Supporting Information). As revealed by single-crystal X-ray diffraction (SCXRD) analysis, the structure of $Ti_{10}Ac_6$ possesses one inversion center (Figure 1a) and crystallizes in a triclinic system with the space group $P\bar{1}$ (Table S1a). $Ti_{10}Ac_6$, in light-yellow, is made up of a dodecahedron-shaped $\{Ti_{10}\}$ metal-oxo core, six Ac ligands, and coordinated HO^{i}Pr and DMF molecules (Figure 1c). As illustrated in Figure S1a, the asymmetric unit of $Ti_{10}Ac_6$ contains five Ti atoms, five μ_3-O atoms, three Ac ligands, five O^{i}Pr, and one DMF solvent molecule. Each of the six-coordinated Ti atoms in the $\{Ti_{10}\}$ core exhibits a slightly distorted octahedral geometry (Figure S1b). The octahedral coordination environment of all Ti atoms consists of six oxygen atoms. However, these oxygen atoms are derived from different coordination groups as shown in Figure S1c. Adjacent Ti atoms are bridged by μ_3-O atoms and Ac ligands to form deca-nucleated TOC (Figure S1d). It is worth noting that the solvent molecules coordinated in the axis of $Ti_{10}Ac_6$ can easily leave and can become potential catalytic active sites.

Structurally, the Ac ligands coordinated to $Ti_{10}Ac_6$ can be replaced by other functionalized ligands in theory, giving rise to a potentially homonuclear isomeric structure. Therefore, to further improve the electron transfer efficiency between the ligand and the titanium-oxo core, the Fc ligands featuring an outstanding redox property and fast charge transfer were introduced to substitute for Ac ligands in the experiment. As expected, Fc ligand decorated $Ti_{10}Fc_8$ (purple-black), with nearly the same dodecahedron-shaped $\{Ti_{10}\}$ core, was successfully synthesized (Figure 1d). The main difference between these two clusters is that $Ti_{10}Fc_8$ is modified by eight Fc ligands, which was due to the substitution of the solvent molecule in the axial direction of the Ti1 atom in $Ti_{10}Ac_6$ by an oxygen atom of the carboxyl group of the Fc ligand. The purple-black $Ti_{10}Fc_8$ belongs to the monoclinic crystal $P2_1/c$ space group confirmed by the SCXRD analysis (Table S1b). As shown in Figure S2a, the asymmetric unit of $Ti_{10}Fc_8$ includes five Ti atoms, six μ_3-O atoms, four Fc ligands, and four FIP solvent molecules. Analogously, all the Ti atoms possess an octahedral coordination environment (Figure S2b), where the Ti1, Ti2, Ti4, and Ti5 atoms were coordinated with μ_3-O atoms, O atoms from Fc ligands, and a coordination solvent molecule, respectively, except that the Ti1 atom is assembled with four μ_3-O atoms and two O atoms from Fc ligands (Figure S2c). Nevertheless, the naked active sites are limited because of much more crowded Fc ligands in $Ti_{10}Fc_8$.

To balance the potential active sites and photosensitivity, Fc and Ac as bifunctionalized ligands were further employed to construct a new dodeca-nuclear $Ti_{12}Fc_2Ac_4$. The SCXRD analysis revealed that $Ti_{12}Fc_2Ac_4$ has the same crystalline system and space group as $Ti_{10}Ac_6$. Interestingly, a nearly identical $\{Ti_{10}\}$ core also can be found in $Ti_{12}Fc_2Ac_4$. Outside the $\{Ti_{10}\}$ dodecahedron skeleton, two additional reversely symmetric Ti atoms (Ti6) are bridged by two μ_2-OEt to form a $\{Ti_{12}\}$ core (Figure 1b). As depicted in Figure 1e, two Fc ligands and four Ac ligands are coordinated to the $\{Ti_{12}\}$ core to form the dodeca-nuclear $Ti_{12}Fc_2Ac_4$ cluster. The asymmetric unit of $Ti_{12}Fc_2Ac_4$ contains two $\{Ti_6\}$ units consisting of six Ti atoms, one μ_4-O atom, five μ_3-O atoms, two μ_2-OEt, one Fc ligand, two Ac ligands, and eight −OEt groups (Figure S3a). Besides, the coordination environment of all Ti atoms is identical to that of $Ti_{10}Ac_6$, except that the axial position of each Ti atom is occupied by an ethanol solvent molecule (Figure S3b). Notably, from the overall structure of $Ti_{12}Fc_2Ac_4$, the Ac ligands originally coordinated to the Ti2 and Ti4 atoms in $Ti_{10}Ac_6$ are replaced by Fc ligands, and the two adjacent Ac ligands connect to Ti4 and Ti5 atoms. Besides, Ti3 and Ti6 atoms are situated on the same side of the $\{Ti_{12}\}$ metal-oxo core, respectively (Figure S3c).

The experimental powder X-ray diffraction (PXRD) patterns of as-synthesized crystal samples were well-matched with the simulated patterns derived from SCXRD data, which demonstrates the high crystallinity and phase purity of $Ti_{10}Ac_6$, $Ti_{10}Fc_8$, and $Ti_{12}Fc_2Ac_4$ samples (Figures S4−S6). Then, these three TOCs were immersed in 0.1 M Na_2SO_4 solution containing 5 ppm 4-CP for 24 h to evaluate their chemical stability. The PXRD patterns before and after soaking are in general accordance, indicating that these three TOCs can maintain structural integrity in Na_2SO_4 solution containing 5 ppm 4-CP. Meanwhile, the thermogravimetric analysis (TGA) was conducted under a nitrogen atmosphere to assess the thermal stability of $Ti_{10}Ac_6$, $Ti_{10}Fc_8$, and $Ti_{12}Fc_2Ac_4$ samples. The corresponding results display that these TOCs have high structural stability below 190 °C (Figure S7). As seen in Figure S8, in the infrared (IR) spectra of $Ti_{10}Ac_6$, $Ti_{10}Fc_8$, and $Ti_{12}Fc_2Ac_4$ samples, the ν(COO) vibrations around 1540 cm^{-1} and 1621−1656 cm^{-1} indicate coordination vibrations of carboxyl groups, respectively. The band at ∼1481 cm^{-1} represents the characteristic band for the Fc fraction. Furthermore, the X-ray photoelectron spectroscopy (XPS) measurements are performed on $Ti_{10}Ac_6$, $Ti_{10}Fc_8$, and $Ti_{12}Fc_2Ac_4$ samples to determine their chemical composition and elemental states. As can be seen from Figures S9−S11, the chemical states of titanium and iron elements in $Ti_{10}Ac_6$, $Ti_{10}Fc_8$, and $Ti_{12}Fc_2Ac_4$ samples featured Ti^{4+} and Fe^{2+}, respectively.[34]

Given the gradual increase in color of the $Ti_{10}Ac_6$, $Ti_{12}Fc_2Ac_4$, and $Ti_{10}Fc_8$ samples, solid-state ultraviolet−visible (UV−vis) absorption spectroscopy was adopted to evaluate their photosensitivity. As shown in Figure 2a, the light absorption range of $Ti_{10}Ac_6$ (light-yellow block crystals) can be extended to near 500 nm. As for $Ti_{12}Fc_2Ac_4$ (tawny-block crystals) in which the Fc ligands are introduced, the visible light absorption range can be increased to 600 nm. $Ti_{10}Fc_8$ (purple-black block crystals) modified with more Fc ligands exhibits a strong and broad absorption band with a maximum absorption of about 620 nm and an extended absorption band up to 800 nm. The excellent UV−vis absorption bands of $Ti_{10}Fc_8$ and $Ti_{12}Fc_2Ac_4$ may be mainly due to the strong charge transfer between high-valence Ti^{4+} ions and electron-donating Fc ligands, which significantly enhances the charge transfer properties of functionalized TOCs.[29,35,36] The electronic structure of $Ti_{10}Fc_8$ was evaluated by DFT calculation to further demonstrate the charge transfer properties of Fc-functionalized titanium-oxo clusters (Figure S12). In addition, the introduced ferrocene groups broaden the visible absorption bands of functionalized TOCs and dramatically reduce their band gaps. As shown in Figure 2b, according to the Kubelka−Munk function, the optical band gaps (E_g) of these TOCs were estimated to be 2.60 ($Ti_{10}Ac_6$), 1.19 ($Ti_{10}Fc_8$), and 1.55 eV ($Ti_{12}Fc_2Ac_4$), respectively. Meanwhile, the energy band distributions of $Ti_{10}Ac_6$, $Ti_{10}Fc_8$, and

https://doi.org/10.1021/jacs.2c11509
J. Am. Chem. Soc. 2023, 145, 6112−6122

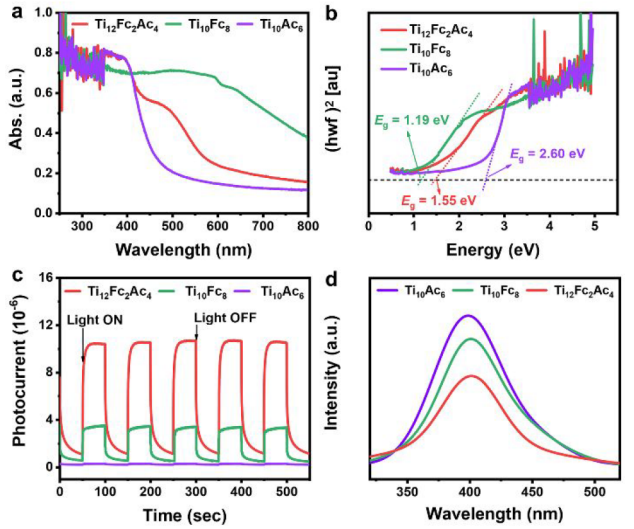

Figure 2. (a) Solid-state UV−vis absorption spectrum of $Ti_{10}Ac_6$, $Ti_{10}Fc_8$, and $Ti_{12}Fc_2Ac_4$ samples. (b) Tauc plots of $Ti_{10}Ac_6$, $Ti_{10}Fc_8$, and $Ti_{12}Fc_2Ac_4$ samples. (c) Transient photocurrent responses of $Ti_{10}Ac_6$, $Ti_{10}Fc_8$, and $Ti_{12}Fc_2Ac_4$ samples under Xe lamp irradiation. (d) Steady-state photoluminescence (PL) spectra of $Ti_{10}Ac_6$, $Ti_{10}Fc_8$, and $Ti_{12}Fc_2Ac_4$ samples.

$Ti_{12}Fc_2Ac_4$ samples were investigated using ultraviolet photoelectron spectroscopy (UPS) (Figures S13−S15).

Based on the strong light-harvesting capacity and intrinsic properties of $Ti_{10}Ac_6$, $Ti_{10}Fc_8$, and $Ti_{12}Fc_2Ac_4$, the transient photocurrent response tests were performed to assess the photogenerated electron−hole pair separation capacities of these TOCs. The photocurrent responses of $Ti_{10}Ac_6$, $Ti_{10}Fc_8$, and $Ti_{12}Fc_2Ac_4$ samples were shown in Figure 2c. A uniform and repeatable photocurrent response was observed when turning on and off the Xe lamp. Especially, the transient photocurrent density of the $Ti_{12}Fc_2Ac_4$ electrode is as great as 3 and 10 times that of the $Ti_{10}Fc_8$ and $Ti_{10}Ac_6$ electrodes, respectively. This demonstrates that $Ti_{12}Fc_2Ac_4$ decorated with bifunctionalized ligands has the best photogenerated electron separation and transfer capacities. Generally, the lower photoluminescence (PL) emission intensity and shorter PL lifetime suggest the more efficient suppression of photoexcited electron−hole pair recombination.[37,38] The PL spectra and PL decay lifetimes of $Ti_{10}Ac_6$, $Ti_{10}Fc_8$, and $Ti_{12}Fc_2Ac_4$ samples were also tested to explore the separation and transfer process of charge carriers (Figures 2d and S17). As shown in Figure 2d, the bifunctionalized $Ti_{12}Fc_2Ac_4$ has a lower emission intensity compared to $Ti_{10}Ac_6$ and $Ti_{10}Fc_8$, which indicates its lower recombination of electron−hole pairs and higher separation efficiency. Besides, electrochemical impedance spectroscopy (EIS) Nyquist plots of $Ti_{10}Ac_6$, $Ti_{10}Fc_8$, and $Ti_{12}Fc_2Ac_4$ samples indicate that the interfacial charge transfer process of $Ti_{12}Fc_2Ac_4$ is faster than that of $Ti_{10}Fc_8$ and $Ti_{10}Ac_6$ (Figure S18). Furthermore, the Hall effect tests were also carried out on $Ti_{10}Ac_6$, $Ti_{10}Fc_8$, and $Ti_{12}Fc_2Ac_4$ samples to determine their carrier mobility, and Table S2 shows that the carrier mobility of $Ti_{12}Fc_2Ac_4$ was 435.88 $cm^2 \cdot v^{-1} \cdot s^{-1}$, which was much higher than that of $Ti_{10}Fc_8$ (185.95 $cm^2 \cdot v^{-1} \cdot s^{-1}$) and $Ti_{10}Ac_6$ (110.31 $cm^2 \cdot v^{-1} \cdot s^{-1}$). Therefore, the $Ti_{12}Fc_2Ac_4$ decorated with bifunctionalized ligands exhibits higher charge separation and transfer efficiency than $Ti_{10}Fc_8$ and $Ti_{10}Ac_6$, which may be beneficial to improve the PEC activity.

In view of the good stability in 0.1 M Na_2SO_4 solution containing 4-CP and thermal stability of the above three coordination clusters, their broad light absorption band, and excellent photogenerated charge separation and transfer efficiency, it is speculated that they have great potential in PEC reactions such as removal of organic pollutants in water. Therefore, the PEC performances of $Ti_{10}Ac_6$, $Ti_{10}Fc_8$, and $Ti_{12}Fc_2Ac_4$ catalysts were investigated in 0.1 M Na_2SO_4 solution containing 5 ppm 4-CP under Xe lamp irradiation in an individual cell with a three-electrode system (a certain concentration of Na_2SO_4 solution as a supporting electrolyte can increase the conductivity of the solution, accelerate the electron migration rate, and thus improve the PEC efficiency) (Figure S19). Initially, the linear sweep voltammograms (LSVs) were performed on $Ti_{10}Ac_6$, $Ti_{10}Fc_8$, and $Ti_{12}Fc_2Ac_4$ catalysts in the presence of 4-CP in the dark and under irradiation, respectively (the applied potential varying from 0 to 1.6 V *vs.* Ag/AgCl). The $Ti_{10}Ac_6$, $Ti_{10}Fc_8$, and $Ti_{12}Fc_2Ac_4$ electrodes show negligible current density under darkness, while the current densities of the three TOC electrodes significantly increase under irradiation (Figures S20−S22). As shown in Figure 3a, the higher anodic photocurrent density is

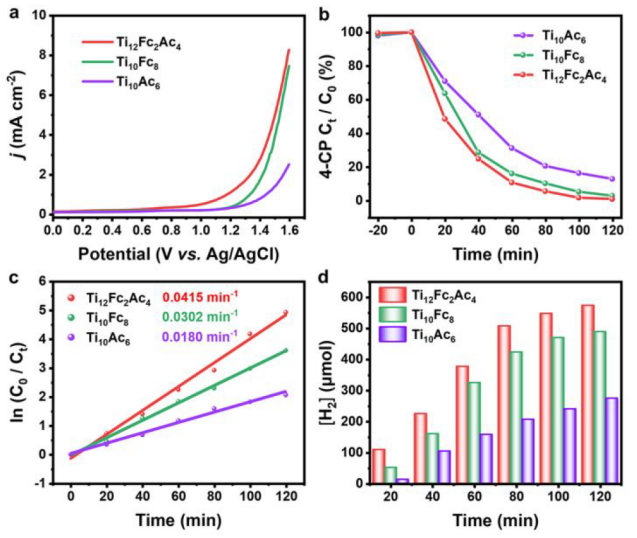

Figure 3. (a) LSV curves of $Ti_{10}Ac_6$, $Ti_{10}Fc_8$, and $Ti_{12}Fc_2Ac_4$ in 0.1 M Na_2SO_4 solution containing 5 ppm 4-CP under the PEC process. (b) The percentage of 4-CP degradation for the PEC degradation process on $Ti_{10}Ac_6$, $Ti_{10}Fc_8$, and $Ti_{12}Fc_2Ac_4$ catalysts. (c) The kinetic plots of $Ti_{10}Ac_6$, $Ti_{10}Fc_8$, and $Ti_{12}Fc_2Ac_4$ catalysts for the 4-CP degradation reaction under Xe lamp irradiation. (d) The yield of H_2 evolution over $Ti_{10}Ac_6$, $Ti_{10}Fc_8$, and $Ti_{12}Fc_2Ac_4$ catalysts during the PEC degradation process of the contaminant 4-CP.

generated for the $Ti_{12}Fc_2Ac_4$ electrode under illumination and increased steeply with increasing potential, which clearly suggests that the $Ti_{12}Fc_2Ac_4$ electrode may have more excellent PEC performance than the other two catalysts in the degradation reaction. Then, the PEC degradation performance of $Ti_{10}Ac_6$, $Ti_{10}Fc_8$, and $Ti_{12}Fc_2Ac_4$ for contaminant 4-CP was studied by the reaction potential of 1.5 V vs Ag/AgCl under the Xe lamp irradiation. The PEC degradation activities of $Ti_{10}Ac_6$, $Ti_{10}Fc_8$, and $Ti_{12}Fc_2Ac_4$ catalysts are shown in Figure 3b, the concentration of 4-CP is decreased rapidly with the degradation time during the PEC degradation process, and it is worth mentioning that $Ti_{12}Fc_2Ac_4$ can degrade 75.33% of

https://doi.org/10.1021/jacs.2c11509
J. Am. Chem. Soc. 2023, 145, 6112−6122

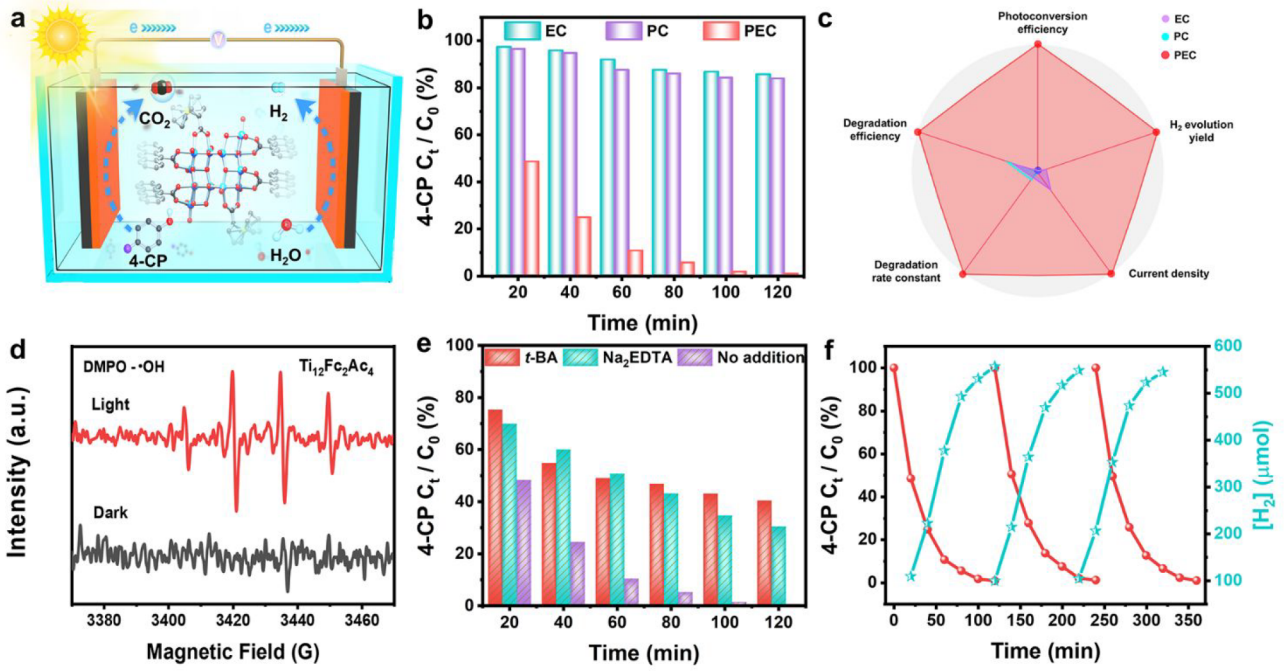

Figure 4. (a) Scheme of the PEC degradation process over the $Ti_{12}Fc_2Ac_4$ catalyst. (b) The performance of the $Ti_{12}Fc_2Ac_4$ catalyst for contaminant 4-CP degradation under EC, PC, and PEC conditions. (c) Radar chart of the performances for the $Ti_{12}Fc_2Ac_4$ catalyst in the EC, PC, and PEC processes, respectively. (d) DMPO spin-trapping EPR spectra of $^{\bullet}OH$ over $Ti_{12}Fc_2Ac_4$ in the dark and on Xe lamp irradiation. (e) Trapping experiments of active oxidation species during PEC degradation of contaminant 4-CP on the $Ti_{12}Fc_2Ac_4$ catalyst. (f) Cycle runs of the $Ti_{12}Fc_2Ac_4$ catalyst for PEC degradation of 4-CP.

4-CP over 40 min, which is faster than $Ti_{10}Fc_8$ (71.49%) and significantly faster than $Ti_{10}Ac_6$ (49.03%). When the PEC degradation was continued for 120 min, the 4-CP was almost completely removed over the $Ti_{12}Fc_2Ac_4$ catalyst with a degradation rate of over 99%, which was higher than the PEC degradation efficiency of 4-CP over $Ti_{10}Fc_8$ (97.28%) and $Ti_{10}Ac_6$ (89.27%) catalysts. To further compare the degradation performance of the three catalysts, the removal kinetics for 4-CP during the PEC process was evaluated by the pseudo-first-order kinetics model, which is approximately fitted with the linear transforms $\ln(C_0/C_t) = kt$ (k is a rate constant). As can be seen in Figure 3c, the degradation rate constant of $Ti_{12}Fc_2Ac_4$ is 0.0415 min^{-1}, which is larger than that of $Ti_{10}Fc_8$ (0.0302 min^{-1}) and $Ti_{10}Ac_6$ (0.0180 min^{-1}). The above results clearly indicate that $Ti_{12}Fc_2Ac_4$ exhibits higher activity among the three catalysts in the PEC degradation of 4-CP.

Besides, the signal of carbon dioxide (CO_2) detected in the gas chromatography (GC) was progressively enhanced with the increase of PEC degradation time, which indicates that the pollutant 4-CP was constantly mineralizing into CO_2 (Figures S23–S25). Therefore, we tried to quantitatively analyze the concentration of CO_2 generated in the reaction system during the PEC degradation of 4-CP by GC (taking $Ti_{12}Fc_2Ac_4$ catalyst as an example) and estimated the theoretical concentration of CO_2 in the reaction system according to the actual concentration of 4-CP. It can be seen from Figure S26 that the CO_2 concentration in the closed reaction system gradually increases with the PEC degradation time. The amount of CO_2 generated by the PEC degradation of 4-CP within 120 min is about 5.64 ± 0.21 μmol over the $Ti_{12}Fc_2Ac_4$ catalyst. Similarly, we also quantified the concentration of Cl^- ions produced in the process of PEC degradation of 4-CP using ion chromatography (IC) (Figure S27). The dechlorination rate with degradation time in the reaction system is shown in Figure S28, and the dechlorination rate of the $Ti_{12}Fc_2Ac_4$ catalyst within 120 min is about 97.2 ± 5.91%, which is close to complete dichlorination.

Apart from the anodic reaction, the cathodic H_2 evolution reaction (HER) performance of $Ti_{10}Ac_6$, $Ti_{10}Fc_8$, and $Ti_{12}Fc_2Ac_4$ catalysts was also investigated and quantified during the PEC degradation processes of the contaminant 4-CP. The H_2 evolution yields of $Ti_{10}Ac_6$, $Ti_{10}Fc_8$, and $Ti_{12}Fc_2Ac_4$ catalysts in 0.1 M Na_2SO_4 solution without and with contaminant 4-CP were studied, respectively (Figures 3d and S29). The results show that the cathodic H_2 production of $Ti_{10}Ac_6$, $Ti_{10}Fc_8$, and $Ti_{12}Fc_2Ac_4$ electrodes gradually increased with increasing PEC time, and the H_2 evolution yield in the 0.1 M Na_2SO_4 solution containing 4-CP was significantly higher than that of without contaminant 4-CP. This indicates that the PEC degradation of pollutants at the photoanode can better facilitate the H_2 evolution reaction at the cathode (Figure 4a).[39] Notably, $Ti_{12}Fc_2Ac_4$ shared a higher H_2 evolution yield (558.86 μmol) with PEC degradation of contaminant 4-CP for 120 min, which was much higher than that of $Ti_{10}Fc_8$ (474.93 μmol) and $Ti_{10}Ac_6$ (267.65 μmol). The results clearly reveal that $Ti_{12}Fc_2Ac_4$ exhibits both excellent PEC pollutant degradation and water splitting activity.

Moreover, some comparative experiments were conducted to further determine the PEC degradation activity of $Ti_{10}Ac_6$, $Ti_{10}Fc_8$, and $Ti_{12}Fc_2Ac_4$ catalysts. Initially, the removal of pollutant 4-CP by $Ti_{10}Ac_6$, $Ti_{10}Fc_8$, and $Ti_{12}Fc_2Ac_4$ catalysts was investigated under photocatalytic (PC, Xe lamp illumination, without applied voltage) and electrocatalytic (EC, darkness, 1.5 V *vs.* Ag/AgCl applied voltage) conditions,

https://doi.org/10.1021/jacs.2c11509
J. Am. Chem. Soc. 2023, 145, 6112−6122

respectively. As illustrated in Figures 4b, S30, and S31, the degradation efficiency of $Ti_{10}Ac_6$, $Ti_{10}Fc_8$, and $Ti_{12}Fc_2Ac_4$ catalysts for 4-CP in the PEC system is much greater than that for the single EC and PC conditions. Moreover, the degradation efficiency of contaminant 4-CP by $Ti_{12}Fc_2Ac_4$ catalyst in 120 min was about 14.38% under the EC condition and 16.16% with the PC treatment. By comparison, the PEC degradation efficiency of $Ti_{12}Fc_2Ac_4$ was evidently superior to that of both EC and PC processes and can reach over 99% in 120 min. Meanwhile, the degradation kinetics of the $Ti_{12}Fc_2Ac_4$ catalyst for 4-CP during the EC, PC, and PEC processes were also evaluated and compared. As seen in Figure S32, the degradation rate constants of 4-CP in the PEC process reach up to 0.0415 min^{-1}, which is 25.93 times that of the PC process (0.0016 min^{-1}) and 29.6 times that of the EC process (0.0014 min^{-1}), respectively. This result obviously indicates that the PEC process was more effective than the PC and EC processes for the degradation of contaminant 4-CP. Meanwhile, the cathodic H_2 production of $Ti_{10}Ac_6$, $Ti_{10}Fc_8$, and $Ti_{12}Fc_2Ac_4$ catalysts was also recorded under PC and EC conditions, respectively (Figures S33−S35). The results show that the H_2 evolution of these three TOCs under PEC conditions is significantly higher than that under PC and EC conditions. The above results clearly demonstrate that the combination of the PC process (the photogenerated charge separation) and EC process (the applied potential) exhibited synergistic effects in the PEC degradation system and then improved the PEC degradation efficiency of contaminant 4-CP and the yield of H_2 evolution (Figure 4c).[40] Besides, the photoconversion efficiency (η) of $Ti_{10}Ac_6$, $Ti_{10}Fc_8$, and $Ti_{12}Fc_2Ac_4$ catalysts was evaluated by the photocurrent as a function of the applied voltage in the PEC cell. The photoconversion efficiencies (η) of $Ti_{12}Fc_2Ac_4$, $Ti_{10}Fc_8$, and $Ti_{10}Ac_6$ electrodes are approximately 0.46%, 0.14%, and 0.03% during the PEC degradation process of 4-CP, respectively.

It is well known that active oxidation species perform a crucial role in the PEC degradation of organic pollutants.[41] The electron paramagnetic resonance (EPR) experiments were carried out to examine the main active oxidation species in the PEC 4-CP degradation reaction. In the EPR experiments, 5,5-dimethyl-1-pyrroline *N*-oxide (DMPO) acted as a free radical scavenger and water was applied as a solvent to generate hydroxyl radicals ($^{\bullet}OH$) in the solution.[42] As depicted in Figures 4d and S36−S38, the characteristic EPR signal is undetected in the dark environment, whereas four significant characteristic peaks are observed under Xe lamp illumination for DMPO-$^{\bullet}OH$ adducts. Meanwhile, the trapping of holes can also be demonstrated by the characteristic EPR signals of 2,2,6,6-tetramethylpiperidine oxide (TEMPOL) (Figure S39).[43] The intensity of the characteristic peak of TEMPOL in the EPR spectrum diminished with light irradiation time, indicating that the concentration of TEMPOL is decreased after reacting with holes. Therefore, the EPR experiment results confirmed the formation of $^{\bullet}OH$ radicals and holes during the PEC degradation of contaminant 4-CP on $Ti_{10}Ac_6$, $Ti_{10}Fc_8$, and $Ti_{12}Fc_2Ac_4$ catalysts.

To further explore the roles of $^{\bullet}OH$ radicals and holes captured in the PEC degradation of 4-CP, a series of quenching experiments were carried out on $Ti_{10}Ac_6$, $Ti_{10}Fc_8$, and $Ti_{12}Fc_2Ac_4$ catalysts. *tert*-Butanol (*t*-BA) and ethylenediaminetetraacetic acid disodium salt (Na_2EDTA) were employed as the scavengers for $^{\bullet}OH$ radicals and holes, respectively.[42] As illustrated in Figure 4e, for $Ti_{12}Fc_2Ac_4$ catalyst, the addition of *t*-BA to the reaction system significantly inhibits the removal of pollutant 4-CP as the degradation efficiency of contaminant 4-CP decreases to 56.70% within 120 min, indicating that $^{\bullet}OH$ is the main reactive oxidation radical in the PEC process. When Na_2EDTA was added to the reaction solution, the removal efficiency decreased to 69.46%, suggesting the generation of holes in the PEC degradation process. Similarly, the active oxidation species generated during the PEC degradation of contaminant 4-CP were also identified by quenching experiments for $Ti_{10}Ac_6$ and $Ti_{10}Fc_8$ catalysts as illustrated in Figures S40 and S41. These results reveal that both $^{\bullet}OH$ radicals and holes play important roles as the main active oxidation species in the PEC degradation process on $Ti_{10}Ac_6$, $Ti_{10}Fc_8$, and $Ti_{12}Fc_2Ac_4$ catalysts.[40]

The stability of the catalyst is an essential criterion for evaluating its reusability and is of great importance for its further application.[19] To investigate the stability of the $Ti_{12}Fc_2Ac_4$ catalyst in the process of PEC degradation of 4-CP, cycling experiments were performed. As shown in Figure 4f, the PEC degradation performance and cathodic HER performance of the $Ti_{12}Fc_2Ac_4$ catalyst did not significantly decrease after three cycles. Moreover, the diffraction peak of PXRD patterns, IR, XPS, and the liquid UV−vis absorption spectrum of the $Ti_{12}Fc_2Ac_4$ catalyst after the PEC degradation reaction confirmed its good structural integrity (Figures S42−S45). Additionally, the inductively coupled plasma emission spectrometer (ICP) and ^1H nuclear magnetic resonance (^1H NMR) spectroscopy analysis of the electrolyte after the PEC degradation reaction further demonstrated that the $Ti_{12}Fc_2Ac_4$ catalyst can remain stable in the PEC degradation of contaminant 4-CP (Table S3 and Figure S46). Besides, the IC results of the electrolyte after the PEC reaction indicated that SO_4^{2-} ions in the electrolyte after reaction did not change (not oxidized) during the PEC reaction, and SO_4^{2-} ions in the electrolyte after the PEC reaction could be well removed by $Ba(OH)_2$ (Figures S47 and S48).

To investigate the differences in PEC degradation performance over $Ti_{10}Ac_6$, $Ti_{10}Fc_8$, and $Ti_{12}Fc_2Ac_4$ catalysts, the concentration of $^{\bullet}OH$ radicals generated in solution was quantified by fluorescence technology using terephthalic acid (TA) as a selective probe reagent.[40,44] The generation of 2-hydroxyterephthalic acid (TAOH produced by TA reacting with $^{\bullet}OH$ radicals) can be detected by excitation at 315 nm with an emission fluorescence of 440 nm (Figure S49). As shown in Figure S50, the TAOH fluorescence intensity gradually increased, indicating the continuous generation of $^{\bullet}OH$ radicals under the PEC degradation process of contaminant 4-CP. Particularly, the $Ti_{12}Fc_2Ac_4$ catalyst exhibits a higher fluorescence intensity of TAOH among these three TOCs, implying the higher generation of $^{\bullet}OH$ radicals in the PEC degradation process of organic contaminant 4-CP. The effective generation of more $^{\bullet}OH$ radicals species on the $Ti_{12}Fc_2Ac_4$ catalyst may be attributed to the efficient photogenerated charge separation and transfer.

In order to further ascertain the PEC degradation reaction mechanism of the contaminant 4-CP on the $Ti_{10}Ac_6$, $Ti_{10}Fc_8$, and $Ti_{12}Fc_2Ac_4$ catalysts, high-performance liquid chromatography (HPLC) and liquid chromatography−mass spectrometry (LC-MS) were used to detect and identify different intermediates (such as hydroquinone (HQ) (Figure S51), benzoquinone (BQ) (Figure S52), 4-chlorocatechol (4-CC) (Figure S53), 1,2,4-trihydroxyphenol (THP) (Figure S54), 4-

https://doi.org/10.1021/jacs.2c11509
J. Am. Chem. Soc. 2023, 145, 6112−6122

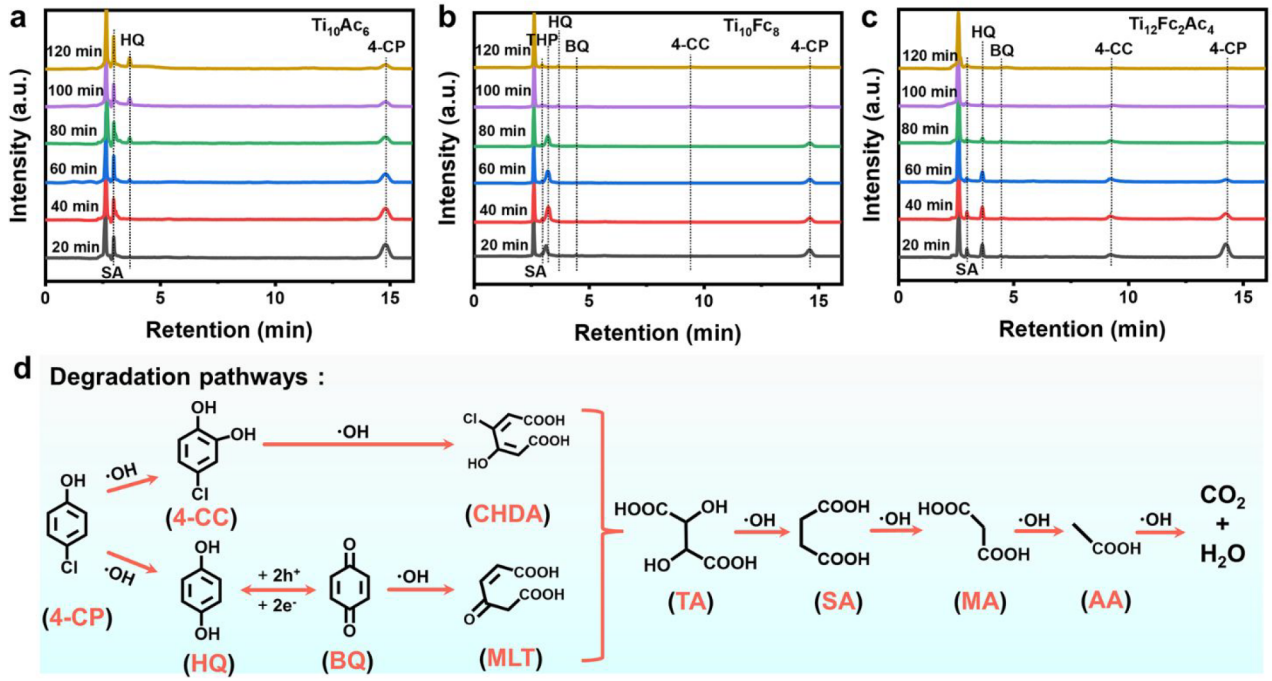

Figure 5. HPLC diagrams of the PEC degradation process of pollutant 4-CP on (a) $\mathbf{Ti_{10}Ac_6}$, (b) $\mathbf{Ti_{10}Fc_8}$, and (c) $\mathbf{Ti_{12}Fc_2Ac_4}$ catalysts. Conditions: MeOH/H_2O = 50:50 (v/v), 1 mL/min, detection wavelength of 280 nm. (d) Proposed degradation pathway of contaminant 4-CP during the PEC degradation on the $\mathbf{Ti_{12}Fc_2Ac_4}$ catalyst. The bottom of the figure presents the abbreviated forms and structural formulas of all intermediates detected by high-performance liquid chromatography (HPLC) and liquid chromatography−mass spectrometry (LC-MS) during the PEC degradation of contaminant 4-CP (4-CP: 4-chlorophenol, 4-CC: 4-chlorocatechol, HQ: hydroquinone, BQ: benzoquinone, CHDA: 3-chloro-4-hydroxyhexa-2,4-dienoic acid, MLT: 4-oxohex-2-enedionic acid, HAD: 3-hydroxyhexa-2,4-dienoic acid, TA: tartaric acid, SA: succinic acid, MA: malonic acid, AA: acetic acid).

oxohex-2-enedionic acid (MLT), 3-hydroxyhexa-2,4-dienoic acid (HDA), tartaric acid (TA), succinic acid (SA) (Figure S55), malonic acid (MA), and acetic acid (AA)) (Figure S56) produced during the PEC degradation process of contaminant 4-CP.[45−47] The results reveal that the three different catalysts generated different intermediates in the PEC degradation of 4-CP. The HPLC spectrum of the PEC degradation of 4-CP on the $\mathbf{Ti_{10}Ac_6}$ catalyst exhibits that only two intermediates, HQ and SA, were observed and that the undegraded 4-CP and HQ were still detected when the reaction was carried out for 120 min (Figure 5a). For the $\mathbf{Ti_{10}Fc_8}$ catalyst, a clear signal of THP, as well as small amounts of intermediates such as 4-CC, HQ, BQ, and SA were detected from the HPLC results (Figure 5b). However, for the $\mathbf{Ti_{12}Fc_2Ac_4}$ catalyst, according to the HPLC results, HQ, BQ, 4-CC, and SA were primarily detected during the degradation of contaminant 4-CP. These four key intermediates initially increased and then gradually decreased with the increase of degradation time. At 120 min, almost no signal was observed for HQ, BQ, and 4-CC, and only a trace amount of SA remained, indicating that all four intermediates were progressively removed (Figure 5c).

Therefore, the degradation pathways of contaminant 4-CP by different catalysts are proposed based on the analysis of the above experimental characterization and the reported literature (Figures 5d, S61, and S62).[6] $\mathbf{Ti_{10}Ac_6}$, $\mathbf{Ti_{10}Fc_8}$, and $\mathbf{Ti_{12}Fc_2Ac_4}$ catalysts generate electron-hole pairs under light irradiation, and the resulting charges were then separated by the voltage application. The photogenerated holes in the anodic catalysts directly react with H_2O molecules to form $^{\bullet}OH$ radicals, which then react with the contaminant. According to the analysis of the HPLC and LC-MS results, there are two possible degradation pathways for PEC degradation of the contaminant 4-CP over the $\mathbf{Ti_{12}Fc_2Ac_4}$ catalyst. One reaction approach is that the $^{\bullet}OH$ radicals attack the neighboring hydroxyl groups of 4-CP to form 4-CC, which can be oxidized by the $^{\bullet}OH$ radical to open the ring to form 3-chloro-4-hydroxyhexa-2,4-dienoic acid (CHDA), then the chloride ion is removed to form TA. The further deep oxidation by $^{\bullet}OH$ radicals forms SA, MA and AA, and finally mineralized to produce CO_2 and H_2O.[48] The other reaction pathway is the $^{\bullet}OH$ radicals attack the opposite OH group of 4-CP, then dechlorinated to form HQ. BQ was produced by a fast electron shuttle mechanism between HQ and BQ,[49] which is oxidized by the $^{\bullet}OH$ radicals to open the ring to form MLT. It is then deeply oxidized by $^{\bullet}OH$ radicals and eventually mineralized to CO_2 and H_2O. Finally, combined with the results of the HPLC tracking experiments on the reaction solution during the PEC degradation of 4-CP and the dechlorination rate of 4-CP over the $\mathbf{Ti_{12}Fc_2Ac_4}$ catalyst, and according to the estimation of CO_2 production in the closed reaction system, the removal rate of total organic carbon in the PEC degradation of 4-CP over the $\mathbf{Ti_{12}Fc_2Ac_4}$ catalyst is about 96.63 ± 3.46% (Figure S63).

Density functional theory (DFT) calculations were employed to understand the difference in the catalytic degradation performance of $\mathbf{Ti_{10}Ac_6}$, $\mathbf{Ti_{10}Fc_8}$, and $\mathbf{Ti_{12}Fc_2Ac_4}$. All molecular structures were optimized with the PBE functional[50] and 6-31G(d) basis set. The solvent effect (H_2O) was included with the solvation model based on the density (SMD) model.[51] All calculations were carried out using the Gaussian 16 C code. Previous reports have shown that a strong interaction of organic pollutants and catalysts plays an

https://doi.org/10.1021/jacs.2c11509
J. Am. Chem. Soc. 2023, 145, 6112−6122

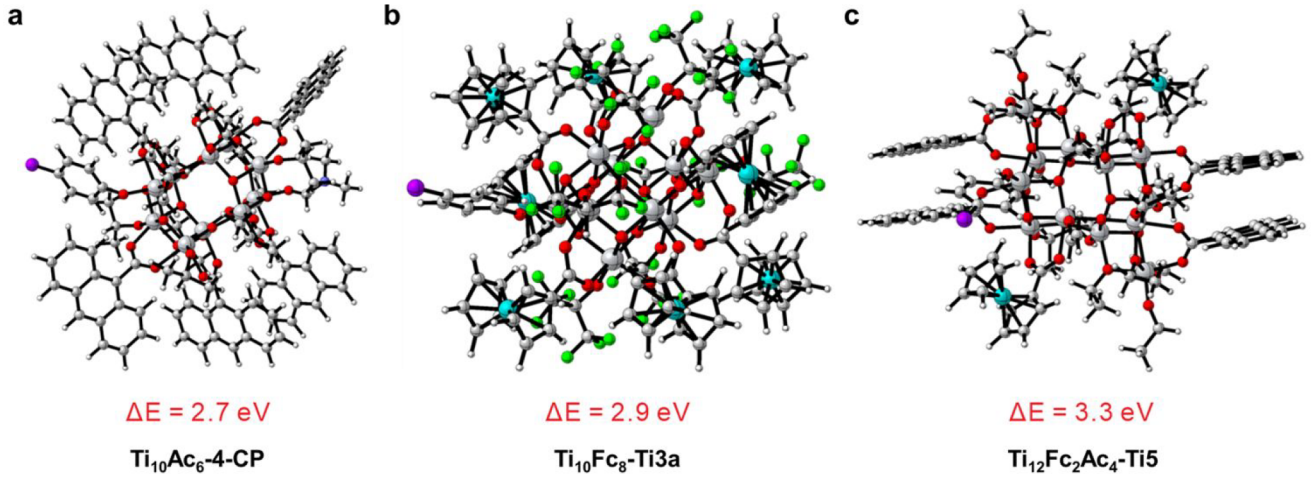

Figure 6. Calculated interaction energy (ΔE) of 4-CP and (a) $Ti_{10}Ac_6$ ($Ti_{10}Ac_6$-4-CP), (b) $Ti_{10}Fc_8$ ($Ti_{10}Fc_8$-Ti3a), and (c) $Ti_{12}Fc_2Ac_4$ ($Ti_{12}Fc_2Ac_4$-Ti5).

important role in achieving a high catalytic degradation performance.[52,53] In view of the complexity of the catalytic process, it is very difficult to accurately study the PEC catalytic reaction mechanism. In order to simplify the treatment, we just tried to judge whether it is one of the factors affecting the performance from the perspective of the interaction energy of the catalyst and 4-CP. To obtain the interactions, we first need to confirm the binding site between catalysts and 4-CP. In $Ti_{10}Ac_6$, we showed that the bond length of the oxygen atom in DMF and the Ti atom is 2.13 Å, which is longer than the bond length (~1.79 Å) of the oxygen atom in HO^{i}Pr and the Ti atom. Generally, a long bond length denotes a small bond energy. In this regard, compared with the HO^{i}Pr group, the DMF molecule is more likely to dissociate. Hence, we obtained the binding structure of $Ti_{10}Ac_6$ and the substrate 4-CP, namely, $Ti_{10}Ac_6$-**4-CP**, by replacing the DMF with deprotonated 4-CP. Based on the $Ti_{10}Ac_6$-**4-CP**, the calculated interaction energy (ΔE) of the substrate 4-CP and $Ti_{10}Ac_6$ is 2.7 eV (Figure 6a). For $Ti_{10}Fc_8$ and $Ti_{12}Fc_2Ac_4$, the dissociable group cannot be screened by the distances of solvent molecules and catalysts because of the similar bond lengths of oxygen atoms in solvent molecules and Ti atoms. For example, the bond lengths are between 1.81 and 1.96 Å in $Ti_{10}Fc_8$ and 1.79−1.83 Å in $Ti_{12}Fc_2Ac_4$. Therefore, we optimized possible binding structures with 4-CP, which are shown in Figures S64 and S65. The more stable binding structures were selected and analyzed. The $Ti_{10}Fc_8$-**Ti3a** and $Ti_{12}Fc_2Ac_4$-**Ti5** structures were extracted for $Ti_{10}Fc_8$ and $Ti_{12}Fc_2Ac_4$, respectively. We showed the ΔE values of 2.9 and 3.3 eV for $Ti_{10}Fc_8$-**Ti3a** and $Ti_{12}Fc_2Ac_4$-**Ti5**, respectively (Figure 6b and c). Based on the results, we concluded that the superb PEC degradation efficiency of $Ti_{12}Fc_2Ac_4$ compared with $Ti_{10}Fc_8$ and $Ti_{10}Ac_6$ may be due to stronger interactions with 4-CP and better hydroxyl radical production. Besides, we also tried to use DFT calculations to simulate the ligand exchange case at the PEB1PBE/6-31G(d) level in Gaussian 16. As shown in Figure S66, the calculation results prove that when DMF, OiPr, OEt, and FIP groups leave after reaction with water, the catalyst structure coordinated with the hydroxyl radical or 4-CP species can still remain structurally stable, which was characterized by vibrational analysis without the presence of imaginary frequencies.

CONCLUSIONS

In summary, three stable TOCs with tunable light-harvesting ability and charge transfer, $Ti_{10}Ac_6$, $Ti_{10}Fc_8$, and $Ti_{12}Fc_2Ac_4$ were synthesized and treated as efficient catalysts to fulfill the cascade reaction of degradation of the organic pollutant 4-CP at the anode and H_2 evolution at the cathode. In contrast to monofunctionalized $Ti_{10}Fc_8$ and $Ti_{10}Ac_6$, bifunctionalized $Ti_{12}Fc_2Ac_4$ balances the light-trapping ability and catalytically active sites effectively. As a result, $Ti_{12}Fc_2Ac_4$ exhibited outstanding PEC activity for the degradation of contaminant 4-CP (degradation efficiency reached over 99% within 120 min), as well as the higher H_2 production (558.86 μmol). Moreover, the PEC degradation process of 4-CP was monitored by HPLC, and the formation of different reaction intermediates was accurately determined. This work presents an important case study and opens up the PEC applications of well-defined crystalline coordination compounds.

ASSOCIATED CONTENT

Supporting Information

The Supporting Information is available free of charge at https://pubs.acs.org/doi/10.1021/jacs.2c11509.

Detailed information regarding the experimental methods, characterization analysis, and DFT calculations (PDF)

Accession Codes

CCDC 2206918−2206920 contain the supplementary crystallographic data for this paper. These data can be obtained free of charge via www.ccdc.cam.ac.uk/data_request/cif, or by emailing data_request@ccdc.cam.ac.uk, or by contacting The Cambridge Crystallographic Data Centre, 12 Union Road, Cambridge CB2 1EZ, UK; fax: +44 1223 336033.

AUTHOR INFORMATION

Corresponding Authors

Jiang Liu − *National and Local Joint Engineering Research Center of MPTES in High Energy and Safety LIBs, Engineering Research Center of MTEES (Ministry of Education), and Key Lab. of ETESPG (GHEI), School of Chemistry, South China Normal University, Guangzhou 510006, China;* orcid.org/0000-0002-2596-4928; Email: liuj0828@m.scnu.edu.cn

https://doi.org/10.1021/jacs.2c11509
J. Am. Chem. Soc. 2023, 145, 6112−6122

Ya-Qian Lan − *National and Local Joint Engineering Research Center of MPTES in High Energy and Safety LIBs, Engineering Research Center of MTEES (Ministry of Education), and Key Lab. of ETESPG (GHEI), School of Chemistry, South China Normal University, Guangzhou 510006, China;* orcid.org/0000-0002-2140-7980; Email: yqlan@m.scnu.edu.cn

Authors

Jing-Jing Liu − *National and Local Joint Engineering Research Center of MPTES in High Energy and Safety LIBs, Engineering Research Center of MTEES (Ministry of Education), and Key Lab. of ETESPG (GHEI), School of Chemistry, South China Normal University, Guangzhou 510006, China*

Sheng-Nan Sun − *National and Local Joint Engineering Research Center of MPTES in High Energy and Safety LIBs, Engineering Research Center of MTEES (Ministry of Education), and Key Lab. of ETESPG (GHEI), School of Chemistry, South China Normal University, Guangzhou 510006, China*

Yi Kuang − *National and Local Joint Engineering Research Center of MPTES in High Energy and Safety LIBs, Engineering Research Center of MTEES (Ministry of Education), and Key Lab. of ETESPG (GHEI), School of Chemistry, South China Normal University, Guangzhou 510006, China*

Jing-Wen Shi − *School of Chemistry and Materials Science, Nanjing Normal University, Nanjing 210023, China*

Long-Zhang Dong − *National and Local Joint Engineering Research Center of MPTES in High Energy and Safety LIBs, Engineering Research Center of MTEES (Ministry of Education), and Key Lab. of ETESPG (GHEI), School of Chemistry, South China Normal University, Guangzhou 510006, China;* orcid.org/0000-0002-9276-5101

Ning Li − *School of Chemical Engineering and Light Industry, Guangdong University of Technology, Guangzhou 510006, China*

Jia-Ni Lu − *School of Chemistry and Materials Science, Nanjing Normal University, Nanjing 210023, China*

Jiao-Min Lin − *National and Local Joint Engineering Research Center of MPTES in High Energy and Safety LIBs, Engineering Research Center of MTEES (Ministry of Education), and Key Lab. of ETESPG (GHEI), School of Chemistry, South China Normal University, Guangzhou 510006, China*

Shun-Li Li − *National and Local Joint Engineering Research Center of MPTES in High Energy and Safety LIBs, Engineering Research Center of MTEES (Ministry of Education), and Key Lab. of ETESPG (GHEI), School of Chemistry, South China Normal University, Guangzhou 510006, China*

Complete contact information is available at: https://pubs.acs.org/10.1021/jacs.2c11509

Author Contributions

J.-J.L. and S.-N.S. contributed equally to this work.

Notes

The authors declare no competing financial interest.

■ ACKNOWLEDGMENTS

This study was financially supported by the NSFC (Grants 92061101, 22271104, 21871141, 21871142, 22071109, and 22225109), the Excellent Youth Foundation of Jiangsu Natural Science Foundation (No. BK20211593), China Postdoctoral Science Foundation (No. 2021M700877), and China Postdoctoral Special Funding Project (No. 2022T150143).

■ REFERENCES

(1) Grant, S. B.; Saphores, J. D.; Feldman, D. L.; Hamilton, A. J.; Fletcher, T. D.; Cook, P. L.; Stewardson, M.; Sanders, B. F.; Levin, L. A.; Ambrose, R. F.; Deletic, A.; Brown, R.; Jiang, S. C.; Rosso, D.; Cooper, W. J.; Marusic, I. Taking the "waste" out of "wastewater" for human water security and ecosystem sustainability. *Science* **2012**, *337* (6095), 681−6.

(2) Wang, C.-C.; Li, J.-R.; Lv, X.-L.; Zhang, Y.-Q.; Guo, G. Photocatalytic organic pollutants degradation in metal−organic frameworks. *Energy Environ. Sci.* **2014**, *7* (9), 2831−2867.

(3) Li, W. W.; Yu, H. Q.; Rittmann, B. E. Chemistry: Reuse water pollutants. *Nature* **2015**, *528* (7580), 29−31.

(4) Grabowska, E.; Reszczynska, J.; Zaleska, A. Mechanism of phenol photodegradation in the presence of pure and modified-TiO_2: A review. *Water Res.* **2012**, *46* (17), 5453−5471.

(5) Gu, Z.; Zhang, Z.; Ni, N.; Hu, C.; Qu, J. Simultaneous Phenol Removal and Resource Recovery from Phenolic Wastewater by Electrocatalytic Hydrogenation. *Environ. Sci. Technol.* **2022**, *56* (7), 4356−4366.

(6) Song, R.; Chi, H.; Ma, Q.; Li, D.; Wang, X.; Gao, W.; Wang, H.; Wang, X.; Li, Z.; Li, C. Highly Efficient Degradation of Persistent Pollutants with 3D Nanocone TiO_2-Based Photoelectrocatalysis. *J. Am. Chem. Soc.* **2021**, *143* (34), 13664−13674.

(7) Xie, M.; Tang, J. C.; Kong, L. S.; Lu, W. H.; Natarajan, V.; Zhu, F.; Zhan, J. H. Cobalt doped g-C_3N_4 activation of peroxymonosulfate for monochlorophenols degradation. *Chem. Eng. J.* **2019**, *360*, 1213−1222.

(8) Long, M.; Long, X.; Zheng, C. W.; Luo, Y. H.; Zhou, C.; Rittmann, B. E. Para-Chlorophenol (4-CP) Removal by a Palladium-Coated Biofilm: Coupling Catalytic Dechlorination and Microbial Mineralization via Denitrification. *Environ. Sci. Technol.* **2021**, *55* (9), 6309−6319.

(9) Lan, S.; Feng, J.; Xiong, Y.; Tian, S.; Liu, S.; Kong, L. Performance and Mechanism of Piezo-Catalytic Degradation of 4-Chlorophenol: Finding of Effective Piezo-Dechlorination. *Environ. Sci. Technol.* **2017**, *51* (11), 6560−6569.

(10) Pi, Y. H.; Li, X. Y.; Xia, Q. B.; Wu, J. L.; Li, Y. W.; Xiao, J.; Li, Z. Adsorptive and photocatalytic removal of Persistent Organic Pollutants (POPs) in water by metal-organic frameworks (MOFs). *Chem. Eng. J.* **2018**, *337*, 351−371.

(11) Lai, T.-L.; Lee, C.-C.; Huang, G.-L.; Shu, Y.-Y.; Wang, C.-B. Microwave-enhanced catalytic degradation of 4-chlorophenol over nickel oxides. *Appl. Catal. B Environ.* **2008**, *78* (1), 151−157.

(12) Kim, J.; Monllor-Satoca, D.; Choi, W. Simultaneous production of hydrogen with the degradation of organic pollutants using TiO_2 photocatalyst modified with dual surface components. *Energy Environ. Sci.* **2012**, *5* (6), 7647−7656.

(13) Xu, L.; Wang, J. Magnetic nanoscaled Fe_3O_4/CeO_2 composite as an efficient Fenton-like heterogeneous catalyst for degradation of 4-chlorophenol. *Environ. Sci. Technol.* **2012**, *46* (18), 10145−53.

(14) Miao, H.; Yang, J.; Peng, G. L.; Li, H. Q.; Zhu, Y. F. Enhancement of the degradation ability for organic pollutants via the synergistic effect of photoelectrocatalysis on a self-assembled perylene diimide (SA-PDI) thin film. *Sci. Bull.* **2019**, *64* (13), 896−903.

(15) Alulema-Pullupaxi, P.; Espinoza-Montero, P. J.; Sigcha-Pallo, C.; Vargas, R.; Fernandez, L.; Peralta-Hernandez, J. M.; Paz, J. L. Fundamentals and applications of photoelectrocatalysis as an efficient process to remove pollutants from water: A review. *Chemosphere* **2021**, *281*, 130821.

(16) Liu, J. C.; Li, J. M.; Li, Y. F.; Guo, J.; Xu, S. M.; Zhang, R. K.; Shao, M. F. Photoelectrochemical water splitting coupled with degradation of organic pollutants enhanced by surface and interface engineering of $BiVO_4$ photoanode. *Appl. Catal. B Environ.* **2020**, *278*, 119268.
(17) Jeon, T. H.; Koo, M. S.; Kim, H.; Choi, W. Dual-Functional Photocatalytic and Photoelectrocatalytic Systems for Energy- and Resource-Recovering Water Treatment. *ACS Catal.* **2018**, *8* (12), 11542−11563.
(18) Rajput, H.; Kwon, E. E.; Younis, S. A.; Weon, S.; Jeon, T. H.; Choi, W.; Kim, K. H. Photoelectrocatalysis as a high-efficiency platform for pulping wastewater treatment and energy production. *Chem. Eng. J.* **2021**, *412*, 128612.
(19) Sun, S.-N.; Dong, L.-Z.; Li, J.-R.; Shi, J.-W.; Liu, J.; Wang, Y.-R.; Huang, Q.; Lan, Y.-Q. Redox-Active Crystalline Coordination Catalyst for Hybrid Electrocatalytic Full Reaction. *Angew. Chem., Int. Ed.* **2022**, *61*, 1−8.
(20) Chen, W.; Liu, S.; Fu, Y.; Yan, H.; Qin, L.; Lai, C.; Zhang, C.; Ye, H.; Chen, W.; Qin, F.; Xu, F.; Huo, X.; Qin, H. Recent advances in photoelectrocatalysis for environmental applications: Sensing, pollutants removal and microbial inactivation. *Coord. Chem. Rev.* **2022**, *454*, 214341.
(21) Garcia-Sanchez, A.; Gomez-Mendoza, M.; Barawi, M.; Villar-Garcia, I. J.; Liras, M.; Gandara, F.; de la Pena O'Shea, V. A. Fundamental Insights into Photoelectrocatalytic Hydrogen Production with a Hole-Transport Bismuth Metal-Organic Framework. *J. Am. Chem. Soc.* **2020**, *142* (1), 318−326.
(22) Xia, Y.-S.; Tang, M.; Zhang, L.; Liu, J.; Jiang, C.; Gao, G.-K.; Dong, L.-Z.; Xie, L.-G.; Lan, Y.-Q. Tandem utilization of CO_2 photoreduction products for the carbonylation of aryl iodides. *Nat. Commun.* **2022**, *13* (1), 2964.
(23) Zhang, M.-M.; Dong, X.-Y.; Wang, Y.-J.; Zang, S.-Q.; Mak, T. C. W. Recent progress in functional atom-precise coinage metal clusters protected by alkynyl ligands. *Coord. Chem. Rev.* **2022**, *453*, 214315.
(24) Yuan, S.-F.; Guan, Z.-J.; Wang, Q.-M. Identification of the Active Species in Bimetallic Cluster Catalyzed Hydrogenation. *J. Am. Chem. Soc.* **2022**, *144* (25), 11405−11412.
(25) Lu, Y.-F.; Dong, L.-Z.; Liu, J.; Yang, R.-X.; Liu, J.-J.; Zhang, Y.; Zhang, L.; Wang, Y.-R.; Li, S.-L.; Lan, Y.-Q. Predesign of Catalytically Active Sites via Stable Coordination Cluster Model System for Electroreduction of CO_2 to Ethylene. *Angew. Chem., Int. Ed.* **2021**, *60* (50), 26210−26217.
(26) Zhang, L.; Li, X.-X.; Lang, Z.-L.; Liu, Y.; Liu, J.; Yuan, L.; Lu, W.-Y.; Xia, Y.-S.; Dong, L.-Z.; Yuan, D.-Q.; Lan, Y.-Q. Enhanced Cuprophilic Interactions in Crystalline Catalysts Facilitate the Highly Selective Electroreduction of CO_2 to CH_4. *J. Am. Chem. Soc.* **2021**, *143* (10), 3808−3816.
(27) Zhang, Q.; Gao, S.; Yu, J. Metal Sites in Zeolites: Synthesis, Characterization, and Catalysis. *Chem. Rev.* **2022**, DOI: 10.1021/acs.chemrev.2c00315.
(28) Li, N.; Liu, J.; Liu, J. J.; Dong, L. Z.; Xin, Z. F.; Teng, Y. L.; Lan, Y. Q. Adenine Components in Biomimetic Metal-Organic Frameworks for Efficient CO_2 Photoconversion. *Angew. Chem., Int. Ed.* **2019**, *58* (16), 5226−5231.
(29) Liu, J.-J.; Li, N.; Sun, J.-W.; Liu, J.; Dong, L.-Z.; Yao, S.-J.; Zhang, L.; Xin, Z.-F.; Shi, J.-W.; Wang, J.-X.; Li, S.-L.; Lan, Y.-Q. Ferrocene-Functionalized Polyoxo-Titanium Cluster for CO_2 Photoreduction. *ACS Catal.* **2021**, *11*, 4510−4519.
(30) Gil-Sepulcre, M.; Garrido-Barros, P.; Oldengott, J.; Funes-Ardoiz, I.; Bofill, R.; Sala, X.; Benet-Buchholz, J.; Llobet, A. Consecutive Ligand-Based Electron Transfer in New Molecular Copper-Based Water Oxidation Catalysts. *Angew. Chem., Int. Ed.* **2021**, *60*, 2−8.
(31) Shima, T.; Zhuo, Q.; Hou, Z. Dinitrogen activation and transformation by multimetallic polyhydride complexes. *Coord. Chem. Rev.* **2022**, *472*, 214766.
(32) Jia, C.; Grace, I. M.; Wang, P.; Almeshal, A.; Huang, Z.; Wang, Y.; Chen, P.; Wang, L.; Zhou, J.; Feng, Z.; Zhao, Z.; Huang, Y.; Lambert, C. J.; Duan, X. Redox Control of Charge Transport in Vertical Ferrocene Molecular Tunnel Junctions. *Chem.* **2020**, *6* (5), 1172−1182.
(33) Xu, M.; Li, D.; Sun, K.; Jiao, L.; Xie, C.; Ding, C.; Jiang, H.-L. Interfacial Microenvironment Modulation Boosting Electron Transfer between Metal Nanoparticles and MOFs for Enhanced Photocatalysis. *Angew. Chem., Int. Ed.* **2021**, *60*, 1−6.
(34) He, Y. P.; Yuan, L. B.; Chen, G. H.; Lin, Q. P.; Wang, F.; Zhang, L.; Zhang, J. Water-Soluble and Ultrastable Ti_4L_6 Tetrahedron with Coordination Assembly Function. *J. Am. Chem. Soc.* **2017**, *139* (46), 16845−16851.
(35) Benedict, J. B.; Coppens, P. The crystalline nanocluster phase as a medium for structural and spectroscopic studies of light absorption of photosensitizer dyes on semiconductor surfaces. *J. Am. Chem. Soc.* **2010**, *132* (9), 2938−44.
(36) Fan, Y.; Li, H. M.; Duan, R. H.; Lu, H. T.; Cao, J. T.; Zou, G. D.; Jing, Q. S. Phosphonate-Stabilized Titanium-Oxo Clusters with Ferrocene Photosensitizer: Structures, Photophysical and Photoelectrochemical Properties, and DFT/TDDFT Calculations. *Inorg. Chem.* **2017**, *56* (21), 12775−12782.
(37) Lu, K.-Q.; Li, Y.-H.; Zhang, F.; Qi, M.-Y.; Chen, X.; Tang, Z.-R.; Yamada, Y. M. A.; Anpo, M.; Conte, M.; Xu, Y.-J. Rationally designed transition metal hydroxide nanosheet arrays on graphene for artificial CO_2 reduction. *Nat. Commun.* **2020**, *11* (1), 5181.
(38) Cai, J.; Huang, J.; Wang, S.; Iocozzia, J.; Sun, Z.; Sun, J.; Yang, Y.; Lai, Y.; Lin, Z. Crafting Mussel-Inspired Metal Nanoparticle-Decorated Ultrathin Graphitic Carbon Nitride for the Degradation of Chemical Pollutants and Production of Chemical Resources. *Adv. Mater.* **2019**, *31* (15), 1806314.
(39) Wu, Z. Y.; Zhou, Z. Y.; Zhang, Y. J.; Wang, J.; Shi, H. J.; Shen, Q.; Wei, G. F.; Zhao, G. H. Simultaneous photoelectrocatalytic aromatic organic pollutants oxidation for hydrogen production promotion with a self-biasing photoelectrochemical cell. *Electrochim. Acta* **2017**, *254*, 140−147.
(40) Koo, M. S.; Cho, K.; Yoon, J.; Choi, W. Photoelectrochemical Degradation of Organic Compounds Coupled with Molecular Hydrogen Generation Using Electrochromic TiO_2 Nanotube Arrays. *Environ. Sci. Technol.* **2017**, *51* (11), 6590−6598.
(41) Liu, Y.; Li, Q.; Lian, Z.; Fan, J.; Tao, Y.; Li, G.; Li, H. Polarization field promoted photoelectrocatalysis for synergistic environmental remediation and H_2 production. *Chem. Eng. J.* **2022**, *437*, 135132.
(42) Li, X.; Huang, X.; Xi, S.; Miao, S.; Ding, J.; Cai, W.; Liu, S.; Yang, X.; Yang, H.; Gao, J.; Wang, J.; Huang, Y.; Zhang, T.; Liu, B. Single Cobalt Atoms Anchored on Porous N-Doped Graphene with Dual Reaction Sites for Efficient Fenton-like Catalysis. *J. Am. Chem. Soc.* **2018**, *140* (39), 12469−12475.
(43) Zhang, J. Q.; Liu, K. N.; Sun, S. L.; Sun, R. C.; Ma, J. L. Photosplitting xylose and xylan to xylonic acid and carbon monoxide. *Green Chem.* **2022**, *24* (21), 8367−8376.
(44) Zhang, X. Y.; Nengzi, L. C.; Li, B.; Liu, L. C.; Cheng, X. W. Design and construction of a highly efficient photoelectrocatalytic system based on dual-Pd/TNAs photoelectrodes for elimination of triclosan. *Sep. Purif. Technol.* **2020**, *235*, 116232.
(45) Bian, W.; Song, X.; Liu, D.; Zhang, J.; Chen, X. The intermediate products in the degradation of 4-chlorophenol by pulsed high voltage discharge in water. *J. Hazard. Mater.* **2011**, *192* (3), 1330−1339.
(46) Barzegar, G.; Jorfi, S.; Zarezade, V.; Khatebasreh, M.; Mehdipour, F.; Ghanbari, F. 4-Chlorophenol degradation using ultrasound/peroxymonosulfate/nanoscale zero valent iron: Reusability, identification of degradation intermediates and potential application for real wastewater. *Chemosphere* **2018**, *201*, 370−379.
(47) Fu, T.; Gong, X.; Guo, J.; Yang, Z.; Liu, Y. Zn-CNTs-Cu catalytic in-situ generation of H_2O_2 for efficient catalytic wet peroxide oxidation of high-concentration 4-chlorophenol. *J. Hazard. Mater.* **2021**, *401*, 123392.
(48) Nie, Y.-C.; Yu, F.; Wang, L.-C.; Xing, Q.-J.; Liu, X.; Pei, Y.; Zou, J.-P.; Dai, W.-L.; Li, Y.; Suib, S. L. Photocatalytic degradation of

organic pollutants coupled with simultaneous photocatalytic H_2 evolution over graphene quantum dots/Mn-N-TiO_2/g-C_3N_4 composite catalysts: Performance and mechanism. *Appl. Catal. B Environ.* **2018**, *227*, 312−321.
(49) Xu, M.; Chen, Y.; Qin, J.; Feng, Y.; Li, W.; Chen, W.; Zhu, J.; Li, H.; Bian, Z. Unveiling the Role of Defects on Oxygen Activation and Photodegradation of Organic Pollutants. *Environ. Sci. Technol.* **2018**, *52* (23), 13879−13886.
(50) Adamo, C.; Barone, V. Toward reliable density functional methods without adjustable parameters: The PBE0 model. *J. Chem. Phys.* **1999**, *110* (13), 6158−6170.
(51) Marenich, A. V.; Cramer, C. J.; Truhlar, D. G. Universal Solvation Model Based on Solute Electron Density and on a Continuum Model of the Solvent Defined by the Bulk Dielectric Constant and Atomic Surface Tensions. *J. Phys. Chem. B* **2009**, *113* (18), 6378−6396.
(52) Zhang, X.; Liu, H.; Li, W.; Cui, G.; Xu, H.; Han, K.; Long, Q. Visible-Light Photocatalytic Degradation of Aromatic Contaminants with Simultaneous H_2 Generation: Comparison of 2,4-Dichlorophenoxyacetic Acid and 4-Chlorophenol. *Catal. Lett.* **2008**, *125* (3−4), 371−375.
(53) Cui, M. S.; Cui, K. P.; Liu, X. L.; Shi, J. P.; Chen, X.; Chen, Y. H. Synergistic effect of mesoporous graphitic carbon nitride and peroxydisulfate in visible light-induced degradation of atenolol: A combined experimental and theoretical study. *Chem. Eng. J.* **2021**, *412*, 127979.

https://doi.org/10.1021/jacs.2c11509
J. Am. Chem. Soc. 2023, 145, 6112−6122